AWARD NUMBER: **W81XWH-14-1-0169**

TITLE: Using Genetic Buffering Relationships Identified in Fission Yeast to Elucidate the Molecular Pathology of Tuberous Sclerosis

PRINCIPAL INVESTIGATOR: **Jim Karagiannis**

CONTRACTING ORGANIZATION: **The University of Western Ontario**
LONDON, ONTARIO, CANADA N6A-5B8

REPORT DATE: **July 2015**

TYPE OF REPORT: **Annual**

PREPARED FOR: **U.S. Army Medical Research and Materiel Command, Fort Detrick, Maryland 21702-5012**

REPORT DOCUMENTATION PAGE

Form Approved
OMB No. 0704-0188

1. REPORT DATE	2. REPORT TYPE	3. DATES COVERED
July 2015	Annual	1 July 2014 - 30 June 2015

4. TITLE AND SUBTITLE
Using Genetic Buffering Relationships Identified in Fission Yeast to Elucidate the Molecular Pathology of Tuberous Sclerosis

5a. CONTRACT NUMBER

5b. GRANT NUMBER
W81XWH-14-1-0169

5c. PROGRAM ELEMENT NUMBER

6. AUTHOR(S)
Jim Karagiannis

E-Mail: jkaragia@uwo.ca

5d. PROJECT NUMBER

5e. TASK NUMBER

5f. WORK UNIT NUMBER

7. PERFORMING ORGANIZATION NAME(S) AND ADDRESS(ES)
THE UNIVERSITY OF WESTERN ONTARIO
1151 RICHMOND ST
LONDON, ONTARIO, CANADA
N6A-5B8

8. PERFORMING ORGANIZATION REPORT NUMBER

9. SPONSORING / MONITORING AGENCY NAME(S) AND ADDRESS(ES)
U.S. Army Medical Research and Materiel Command
Fort Detrick, Maryland 21702-5012

10. SPONSOR/MONITOR'S ACRONYM(S)

11. SPONSOR/MONITOR'S REPORT NUMBER(S)

12. DISTRIBUTION / AVAILABILITY STATEMENT
Approved for Public Release; Distribution Unlimited

13. SUPPLEMENTARY NOTES

14. ABSTRACT
Using the genetically tractable fission yeast as a model, we sought to exploit recent advances in gene interaction biology to identify novel drug targets for use in the fight against tuberous sclerosis. Our ongoing study has identified two genes, *fft3* (a SMARCAD1 family ATP-dependent DNA helicase) and *ypa1* (a PTPA family protein phosphatase) as excellent candidates for continued analysis. While deletion of either gene has little phenotypic effect in normal cells, their loss in either *tsc1* or *tsc2* mutants profoundly inhibits growth. Thus, inhibition of either *fft3* or *ypa1* may represent an "Achilles' heel" of cells defective in hamartin or tuberin function. In addition, due to the fact that our work necessitated the ability to unambiguously compare genetic interactions, we developed a formal and general mathematical framework for the quantitation of genetic buffering strength. This methodology was recently published and is freely available to the public at "www.mathematica-journal.com/2015/03/the-quantitation-of-non-classical-buffering/".

15. SUBJECT TERMS
Tuberous Sclerosis, Genetic Buffering, Fission Yeast, Recombinase-Mediated Cassette Exchange, PTPA family protein phosphatase, ATP-dependent DNA Helicase

16. SECURITY CLASSIFICATION OF:			17. LIMITATION OF ABSTRACT	18. NUMBER OF PAGES	19a. NAME OF RESPONSIBLE PERSON
a. REPORT	b. ABSTRACT	c. THIS PAGE			USAMRMC
Unclassified	Unclassified	Unclassified	Unclassified	44	19b. TELEPHONE NUMBER *(include area code)*

TABLE OF CONTENTS

1. INTRODUCTION

Tuberous sclerosis complex (TSC) is an inherited disorder characterized by the appearance of benign tumors in the brain, heart, lung, kidney, eyes, and/or skin. The disease affects as many as 40,000 individuals in the United States and is caused by mutations in one of two genes, *TSC1* (encoding a protein called hamartin), and *TSC2* (encoding a protein called tuberin). While research of the past two decades has provided a wealth of information regarding the genetic origins of TSC, the complexity of the molecular pathways involved, together with their intricate temporal and spatial interactions, has made it difficult to elucidate the full molecular pathology of the disease. Fortunately, recent technical and conceptual advances with respect to the importance of "genetic buffering" on phenotypic variation have provided novel avenues of exploration regarding this goal.

Using the genetically tractable fission yeast as a model, our USAMRAA funded research has sought to exploit recent advances in genetic interaction network biology to analyze previously uncharacterized genes that modulate the phenotypic effects of hamartin and tuberin loss of function mutations. Of particular interest are genes displaying negative genetic interactions with either *tsc1* or *tsc2*. Since tumor formation in TSC patients arises from loss of heterozygosity, this characteristic identifies the human orthologs of these genes as potential therapeutic targets i.e. drugs inhibiting a negative interactor would presumably suppress only the growth of tumor cells (which bear two mutant copies of the affected TSC gene: the inherited mutant germline copy, and the copy affected by the "second-hit") while leaving phenotypically normal cells (carrying only the mutant germline copy) unaffected.

Our research of the past year has clearly identified two genes, *fft3* (encoding a SMARCAD1 family ATP-dependent DNA helicase) and *ypa1* (encoding a PTPA family protein phosphatase) as excellent candidates for continued analysis. While deletion of either gene has little phenotypic effect in normal cells, their loss in either *tsc1* or *tsc2* mutant backgrounds profoundly inhibits growth. Thus, inhibition of either *fft3* or *ypa1* may represent an "Achilles' heel" of cells defective in hamartin or tuberin function. Importantly, both of these genes have clear orthologs in humans.

In addition to our bench-top analyses, we have also developed a formal mathematical methodology for the quantitation of genetic buffering strength (this was necessitated by the need for a system that could be used to unambiguously compare genetic interaction data). This methodology provides a simple, general, and rigorous mathematical paradigm with which to exactly quantitate the buffering strength of any genetic determinant. The methodology was recently published in the peer-reviewed "*The Mathematica Journal*" and is freely available to the public at "www.mathematica-journal.com/2015/03/the-quantitation-of-non-classical-buffering/".

2. KEYWORDS

Tuberous Sclerosis, Genetic Buffering, Fission Yeast, Recombinase-Mediated Cassette Exchange, PTPA family protein phosphatase, ATP-dependent DNA Helicase

3. ACCOMPLISHMENTS

Our research accomplishments of the last year are described below in the context of the Specific Aims outlined in the approved Statement of Work (SOW).

SPECIFIC AIM 1: Establish an *S. pombe* model of TSC by replacing the endogenous *S. pombe* hamartin and tuberin genes with human *TSC1* and *TSC2*, respectively.

Task 1: Create tsc1::ura4$^+$ and tsc2::ura4$^+$ "base" strains.

Predicted Completion Date: August 31st, 2014

Progress: Gene deletion cassettes for both the *tsc1* and *tsc2* genes were created by PCR amplifying the *ura4*$^+$ selectable marker (together with the *loxP* and *loxM3* recombination sites) from the pAW1 vector using primers oTsc11 (5'-tta tca atg ctg cca aga ctt gct atc agt ata atg tcg cat agt tgt ata tca acg ttg act ttg cca act ttg tac gac gga tcc ccg ggt taa tta a-3'), and oTsc12 (5'-aat tat ttt ata tgg aat gag caa gta tgt ttt atc ata att gac cag ttc att tca agg acc ttc aaa aat ata cct acg aat tcg agc tcg ttt aaa c-3'), or oTsc13 (5'-tta aga gtt cag att tgc ttt atg tgg tta ttc tgc tga agg tcc taa ttt att gac gtt gaa aaa taa agg cca cat agc gga tcc ccg ggt taa tta a-3'), and oTsc14 (5'-ata aaa aaa att aat taa tga tgg caa ggc aca atc gta atc aat ctt tta att tag gac ttt tta tat gcc ctt atg gcg aat tcg agc tcg ttt aaa c-3'), respectively. Strain ED666 (*ura4-D18 leu1-32 ade6-210 h*$^+$) was then transformed with either the *tsc1* specific or *tsc2* specific cassette. Ura$^+$ transformants were isolated and the respective gene deletions confirmed by colony PCR using primers oTsc15 (5'-atg tgg cag act acg cta tcc t-3') and oTsc17 (5'-atg ctt ccc cta att cat agc a-3') for the *tsc1* deletion, and oTsc16 (5'-agc aac cta cga gag gaa gat g-3') and oTsc18 (5'-gcg cat aac cct ttc tac att c-3') for the *tsc2* deletion.

Status: Complete.

Task 2: Obtain full length cDNA clones of human *TSC1* (Accession BC167824) and *TSC2* (Accession BC150300) from ThermoScientific. PCR amplification.

Predicted Completion Date: August 31st, 2014

Progress: Recent advances in DNA synthesis technology altered our strategy with respect to the original SOW document (see Section 5: Problems/Changes). Instead of purchasing cDNA clones and using standard amplification/cloning techniques, it proved more economical (in terms of both time and money) to synthesize the desired sequences. Full length clones were thus obtained through Genscript's DNA synthesis service. All constructs were confirmed by DNA sequencing.

Status: Complete.

Task 3: Molecular cloning of *TSC1* and *TSC2* into "exchange" plasmids.

Predicted Completion Date: September 30th, 2014

Progress: As part of the service provided by Genscript, it was possible to have the synthetic sequences cloned directly into the pAW8X "exchange" plasmids upon synthesis.

Status: Complete.

Task 4: Transform exchange plasmids into *S. pombe* strain ED666. Select for clones that have exchanged the *ura4*$^+$ cassette with *TSC1*/*TSC2*. Verify genotypes by colony PCR.

Predicted Completion Date: October 31st, 2014

Progress: The *tsc1::ura4/tsc2:ura4* base strains were transformed with the pAW8X-TSC1/pAW8X-TSC2 vectors containing the human *TSC1* and *TSC2* genes. As controls, the base strains were also transformed with the pAW8X-tsc1 and pAW8X-tsc2 vectors containing the fission yeast *tsc1* and *tsc2* genes. Cells in which the *ura4*$^+$ gene was exchanged with *TSC1*/*TSC2*/*tsc1*/*tsc2* were selected by growth on media containing 5-fluoroorotic acid (a drug counter selectable to Ura$^+$ cells). This created strains in which human *TSC1* or *TSC2,* or fission yeast *tsc1* or *tsc2*, were expressed from the endogenous fission yeast *tsc1/tsc2* promoters at the native *tsc1/tsc2* loci. These strains have been denoted as *tsc1::TSC1*^{Hs}*, tsc2::TSC2*^{Hs}*, tsc1::tsc1*^{Sp}, and *tsc2::tsc2*^{Sp}. Strains bearing both substitutions were then created by crossing *tsc1::TSC1*^{Hs} and *tsc2::TSC2*^{Hs} strains of opposite mating type and screening progeny by colony PCR to identify *tsc1::TSC1*^{Hs} *tsc2::TSC2*^{Hs} cells. A complete catalog of strains created during the course of this work appears in Section 6.5.1, Research Material.

Status: Complete.

Task 5: Complementation Assays.

Predicted Completion Date: December 31st, 2014

Progress: The ability of human *TSC1/TSC2* to complement the loss of the fission yeast *tsc1/tsc2* genes was determined by assaying the growth of wild-type, *tsc1Δ*, *tsc2Δ*, *tsc1::TSC1*^{Hs}*, tsc2::TSC2*^{Hs}*, tsc1::TSC1*^{Hs} *tsc2::TSC2*^{Hs}, *tsc1::tsc1*^{Sp}, and *tsc2::tsc2*^{Sp} strains on minimal media containing 60 μg/ml of canavanine. As expected *tsc1Δ* and *tsc2Δ* base strains, unlike wild-type controls, were resistant to the drug and were able to form colonies. Also as expected, *tsc1::tsc1*^{Sp} and *tsc2::tsc2*^{Sp} strains behaved as wild type and were unable to form colonies (indicating that the recombinase mediated cassette exchange methodology correctly integrated the synthetic constructs). Unfortunately, *tsc1::TSC1*^{Hs}, *tsc2::TSC2*^{Hs}, as well as *tsc1::TSC1*^{Hs} *tsc2::TSC2*^{Hs} strains were able to form

colonies (indicating that the expression of the human orthologs was incapable of complementing the loss of the fission yeast *tsc1* and *tsc2* genes).

Status: Complete.

SPECIFIC AIM 2: Create "*TSC* mutant allele" array.

Task 1: Construction of TSC mutant alleles via direct synthesis or site-directed mutagenesis techniques.

Predicted Completion Date: February 28th, 2015

Progress: As discussed above, due to the lack of complementation, the remainder of the project will be conducted using the fission yeast *tsc1* and *tsc2* genes. To this end, site-directed mutagenesis was employed to incorporate a total of five mutations into the *tsc2* gene. Each of these mutations (G296E, R927W, N1199S, P1223L, R1296P) affects residues analogous to mutations identified clinically. New England Biolab's Q5 Site-Directed Mutagenesis Kit was used to generate pUC57-tsc2_G296E, pUC57-tsc2_R927W, pUC57_N1199S, pUC57_P1223L, and pUC57_R1296P plasmids. DNA sequence analysis confirmed the incorporation of the desired changes. The same strategy will be used to create a similar panel of *tsc1* mutant alleles.

Status: In Progress (50% Complete).

Task 2: Molecular cloning of mutant alleles into exchange plasmids.

Predicted Completion Date: March 31st, 2015

Progress: As of June 30th, 2015, two of the clones (pUC57-tsc2_G296E, and pUC57_N1199S) have been cloned into the pAW8X exchange plasmids using the *XhoI* and *SacI* restriction sites and standard molecular techniques. Cloning of the remaining constructs is in progress.

Status: In Progress (20% Complete).

Task 3: Transform exchange plasmids into S. pombe strain ED666. Select for clones that have exchanged the *ura4*$^+$ cassette with TSC1/TSC2. Verify genotypes by colony PCR.

Predicted Completion Date: April 31st, 2015

Progress: Upon completion of Task 2 (above), recombinase mediated cassette exchange will be used to integrate the respective mutant *tsc1* and *tsc2* alleles into the appropriate base

strains.

Status: Pending Completion of Task 2.

Task 4: Confirm lack of complementation.

Predicted Completion Date: June 30th, 2015

Progress: Upon completion of Tasks 2 and 3 (above), complementation assays based on canavanine resistance will be performed as described in Specific Aim 1, Task 5.

Status: Pending Completion of Tasks 2 and 3.

SPECIFIC AIM 3: Intercross strains of the TSC mutant allele panel with strains of the "putative interactor" panel.

Task 1: Intercross "TSC mutant allele" array with "interactor" panel.

Predicted Completion Date: October 31st, 2015

Progress: Control experiments in which the fission yeast interactor panel was crossed to either the *tsc1Δ* or *tsc2Δ* gene deletion mutants have been completed. These control experiments are crucial in that they will provide a proper baseline of comparison for future assays conducted with the TSC mutant allele panels. Due to the confounding effect of auxotrophic markers present in the interactor panel (derived from the Bioneer gene deletion set), it was necessary to construct an alternative panel of strains devoid of secondary genetic alterations (see Section 5: Problems/Changes). Intercrossing of the *tsc1* and *tsc2* mutant allele panels will be performed upon completion of Specific Aim 2.

Status: In Progress (30% Complete).

Task 2: Isolation of double mutant progeny. Growth Assays.

Predicted Completion Date: October 31st, 2015

Progress: Control assays (in triplicate) comparing the growth of wild type, *tsc1Δ*, *tsc2Δ*, the interactor panel mutants, as well as the respective double mutants have been completed. Briefly, a micromanipulator was used to array single cells representing each genotype (in quadruplicate) upon YES agar plates. Plates were incubated at 30°C for five days. Digital images were taken at 24 hour intervals. These experiments identified *fft3* (a SMARCAD1 family ATP-dependent DNA helicase) and *ypa1* (a PTPA family protein phosphatase) as strong negative interactors of both the *tsc1Δ* and *tsc2Δ* gene deletions (see Section 4.1, Impact). Representative images of plates at day 4 for one biological replicate are shown

below (10-27 denotes the *ypa1Δ* mutant, and 30-77 denotes the *fft3Δ* mutant). Growth assays using the *tsc1* and *tsc2* mutant allele panels will be performed upon completion of Specific Aim 2.

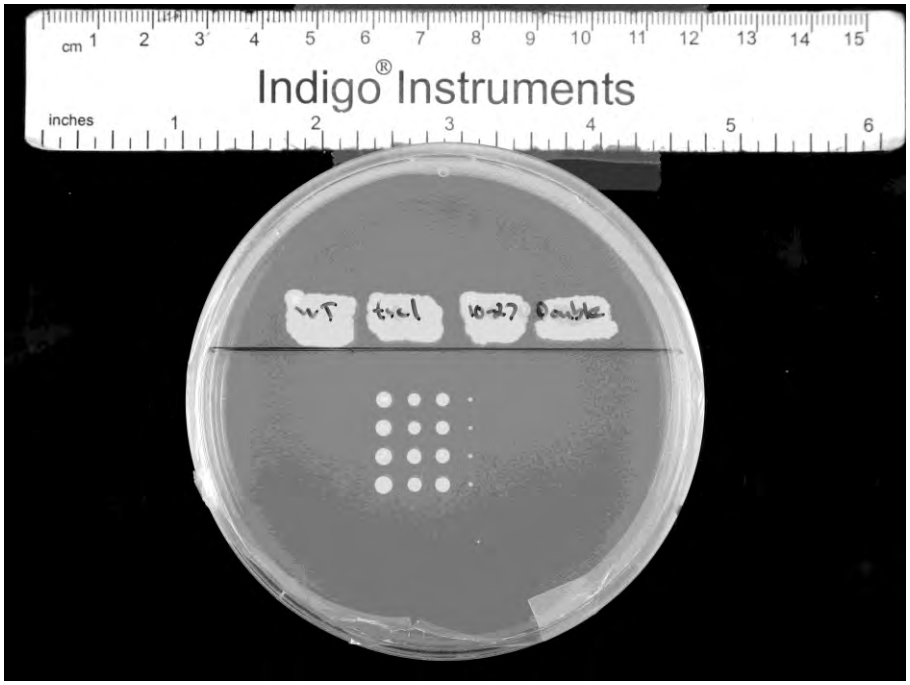

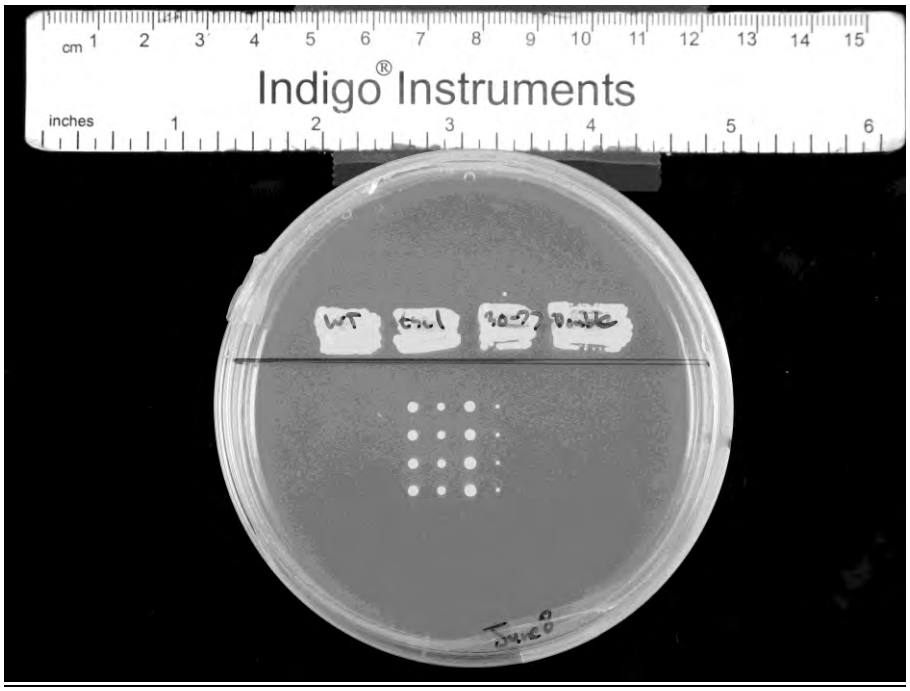

Status: In Progress (30% Complete).

Task 3: Image analysis of colony size.

Predicted Completion Date: December 31st, 2015

Progress: ImageJ (imagej.nih.gov/ij/) analysis tools were used to determine the colony size of wild type, *tsc1Δ*, *tsc2Δ*, each interactor panel mutant, and the respective double mutants (in quadruplicate) for each of three independent biological replicates. Representative data describing the interaction between *tsc1* and either *ypa1* or *fft3* is shown below.

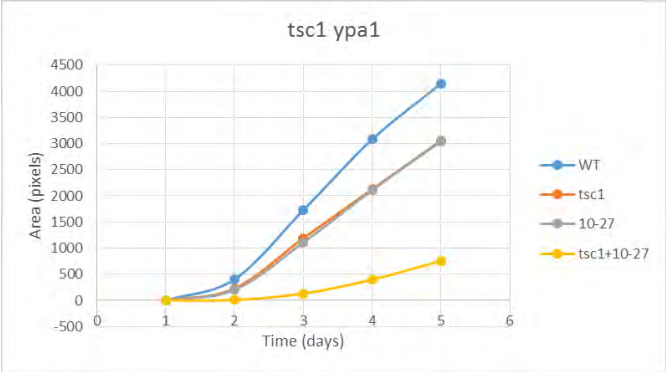

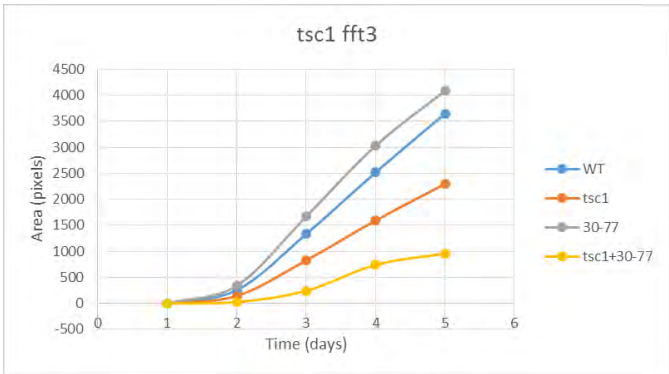

Status: In Progress (30% Complete).

SPECIFIC AIM 4: Physiological analysis of TSC modifiers

Task 1: Test effect of pharmacological inhibitors of "negative" interactors (if available) in strains expressing wild-type and mutant TSC alleles.

Predicted Completion Date: February 28th, 2016

Progress: These assays will be performed upon completion of Specific Aims 2 and 3.

Status: Pending Completion of Specific Aims 2 and 3.

Task 2: Molecular/physiological/genetic analysis of interactors. Specific analyses will be determined based on the molecular identity of the genes identified from the interactor panel.

Predicted Completion Date: June 30th, 2016

Progress: These assays will be performed upon completion of Specific Aims 2 and 3.

Status: Pending Completion of Specific Aims 2 and 3.

4. IMPACT

4.1 Impact on the Development of the Principal Disciplines of the Project

Our ongoing study has clearly identified *fft3* (a SMARCAD1 family ATP-dependent DNA helicase) and *ypa1* (a PTPA family protein phosphatase) as strong negative interactors of both the *tsc1Δ* and *tsc2Δ* gene deletions. While deletion of either gene has little phenotypic effect in normal cells, their loss in either *tsc1* or *tsc2* mutants profoundly inhibits growth. Thus, the chemical inhibition of the encoded Fft3 or Ypa1 proteins (both of which have clear orthologs in humans) may represent a novel means with which to specifically inhibit the growth of cells defective in hamartin or tuberin function. In other words, the inhibition of either Fft3 or Ypa1 may represent an "Achilles' heel" of cells diminished in *tsc1* or *tsc2* activity. It is important to note that neither of these genes have been identified using traditional genetic analysis. Thus, their continued study represents a novel avenue of exploration with regards to the molecular pathology of TSC.

4.2 Impact on other Disciplines

During the course of analyzing our genetic interaction data, it became apparent that there was no established method with which to formally and unambiguously quantitate the strength of "genetic buffering". To address this issue we developed a formal, axiomatic methodology – using the Wolfram Programming Language – to achieve this goal. The method is described in our recent publication "The Quantitation of Non-Classical Buffering: Applying the Formal and General Approach to Problems in the Biological Sciences (included in this report as Appendix A and freely available at "www.mathematica-journal.com/2015/03/the-quantitation-of-non-classical-buffering/". While we will use this methodology to quantitate and compare the genetic interactions observed between the interactor panel and TSC mutant allele array, the methodology can also be applied to any scenario (and in any discipline) where a quantity partitions between two compartments or states.

4.3 Impact on Technology Transfer

Nothing to Report

4.4 Impact on Society Beyond Science and Technology

Nothing to Report.

5. CHANGES/PROBLEMS

5.1 Changes in Approach

5.1.1. Cloning of human *TSC1* and *TSC2*

Instead of purchasing cDNA clones of *TSC1* and *TSC2* and subsequently employing standard amplification and cloning techniques to create the exchange plasmids, we chose to use a commercial entity to synthesize the desired sequences. Recent advances in DNA synthesis technology have made such direct DNA synthesis approaches the most economical choice. Full length clones were thus obtained through Genscript's DNA synthesis service.

5.1.2. TSC mutant allele panel

Unfortunately, human *TSC1* or *TSC2* were unable to complement the loss of their fission yeast counterparts when expressed at the native *tsc1* or *tsc2* loci. While disappointing, this was an eventuality we previously considered. As discussed in the original project narrative (page 4, paragraph 1), the project will continue using the fission yeast hamartin/tuberin genes instead of their human orthologs. This is to say alleles of the fission yeast *tsc1* and *tsc2* genes – bearing mutations affecting residues analogous to those identified clinically – will be employed.

5.2 Actual or Anticipated Problems

5.2.1 Confounding Effect of Auxotrophic Markers

Due to the confounding effect of auxotrophic markers present in the interactor panel (derived from the Bioneer gene deletion set), it was necessary to construct an alternative panel devoid of secondary genetic alterations. This delayed the initiation of Specific Aims 2 and 3. While tedious and time consuming an alternative interactor panel, devoid of any background auxotrophic markers, has now been constructed and will be employed during the remainder of the study.

5.2.2 Personnel

The initial proposal identified graduate student, Bidhan Chakraborty, as associated with the project. Unfortunately, Mr. Chakraborty, upon successfully defending his MSc thesis, returned to Bangladesh to be married and ultimately decided to pursue other interests. While Mr. Chakraborty has now been replaced by Mr. Ryan Chevalier, his initial departure caused minor delays with respect to the completion of Specific Aim 2. These manpower issues have now been resolved and we expect no further difficulties.

6. PRODUCTS

6.1 Publications, Conference Papers, and Presentations

6.1.1 *Journal Publications*

Karagiannis J. The Quantitation of Non-Classical Buffering: Applying the Formal and General Approach to Problems in the Biological Sciences. *The Mathematica Journal* **17**, 2015. (Published)

6.1.2 *Books or Other Non-Periodical, One-time Publications*

Nothing to Report

6.1.3 *Other Publications, Conference Papers, and Presentations*

Nothing to Report

6.2 Websites or Other Internet Sites

Nothing to Report

6.3 Technologies or Techniques

Nothing to Report

6.4 Inventions, Patent Applications, and/or Licenses

Nothing to Report

6.5 Other Products

6.5.1 *Research Material (Fission Yeast Strains)*

Genotypes of the relevant fission yeast strains generated during the course of this study are listed below:

- *tsc1Δ* "base" strain (gene deletion with flanking *loxP* and *loxM3* sites)
- *tsc2Δ* "base" strain (gene deletion with flanking *loxP* and *loxM3* sites)
- *tsc1::tsc1*^{Sp}
- *tsc2::tsc2*^{Sp}
- *tsc1::TSC1*^{Hs}
- *tsc2::TSC2*^{Hs}
- *tsc1::TSC1*^{Hs}*tsc2::TSC2*^{Hs}

7. PARTICIPANTS

Name:	Jim Karagiannis
Nearest Person Month Worked:	12
Contribution to Project:	Principal Investigator
Name:	Ryan Chevalier
Nearest Person Month Worked	4
Contribution to Project	Mr. Chevalier was involved in the routine growth and maintenance of fission yeast cultures, molecular cloning, and was also responsible for all image analysis of genetic interaction data.

8. SPECIAL REPORTING REQUIREMENTS

Not Applicable

The Mathematica® Journal

The Quantitation of Non-classical Buffering

Applying the Formal and General Approach to Problems in the Biological Sciences

Jim Karagiannis

A formal, axiomatic conceptualization of buffering action—generally applicable to any physical, chemical, or biological process—was first presented by B. M. Schmitt in 2005 [1, 2]. This article provides a series of tools designed to aid in the application of these concepts to both classical and non-classical buffering phenomena. To illustrate the utility of the approach in the biological sciences, an abstract measure of the magnitude of "genetic" buffering associated with an allele of the gene encoding the heat shock protein Hsp90 is determined.

Introduction

Buffering is observed when a parameter changes less than expected in response to a given disturbance. For example, if a strong acid is added to an aqueous solution, and not all of the added H^+ ions remain free (unbound), then the solution is said to act as a buffer. While such phenomena have been observed in the physical, chemical, and biological sciences for centuries, a formal and general approach for their quantitation across distinct disciplines was not presented until recently [1, 2].

In [1, 2], B. M. Schmitt presents a comprehensive mathematical framework for evaluating buffering action—a framework that is applicable to any scenario in which a quantity partitions between two compartments or states. While suitable for the analysis of "classical" buffering phenomena (e.g. acid-base chemistry), the formalism also provides a simple means with which to quantitate and characterize phenomena that, at first glance, seem to be outside the buffering paradigm—at least when the term is used in its traditional sense with respect to the homeostasis of physiological parameters (see [2] for several in-depth examples of the formal and general approach applied to phenomena spanning diverse disciplines).

This article provides a series of mathematical tools designed to facilitate the application of Schmitt's paradigm to both "classical" and "non-classical" buffering phenomena. By inputting the transfer function $\tau(x)$ and the buffering function $\beta(x)$, the provided code:

(1) defines the four buffering parameters *t*, *b*, *T*, and *B*; (2) provides a series of graphical outputs describing the system; and (3) calculates the buffering angle α, thereby classifying the system as being moderating/amplifying/inverting/non-inverting. Thus, the burden of computation associated with the approach is seamlessly transferred from the user to the *Mathematica* kernel.

Lastly, in order to illustrate the utility of the approach outside traditional disciplines, I use these same tools to calculate the magnitude of "genetic" buffering associated with an allele of the gene encoding the heat shock protein Hsp90. In this way, the capacity of an allele to buffer phenotypic variation is formally and quantitatively determined for the first time.

An Intuitive, Linear Example Based on the Partitioning of Fluids in Communicating Vessels

To illustrate Schmitt's "formal and general approach," consider a system comprised of a pair of communicating vessels (i.e. cylindrical flasks connected by a small tube). As described in [1], the total volume of liquid in the vessels, *x*, is the sum of the two partial volumes contained in each vessel. In the specific example described below, the rightmost of the two cylindrical vessels (the "buffering" vessel) has a radius exactly two times that of the first. Thus, any fluid added to the leftmost vessel (the "transfer" vessel) will partition in a ratio of 1:4 between the transfer and buffering vessels. The partial volume present in the transfer vessel is thus one-fifth the total volume of fluid added to the system. Likewise, the partial volume present in the buffering vessel is four-fifths the total volume of fluid added to the system.

```
Graphics3D[{
  Cylinder[{{0, 0, 0}, {0, 0, 5}}, 0.5],
  Cylinder[{{3, 0, 0}, {3, 0, 5}}, 1],
  Cylinder[{{0.1, 0.1, 0.1}, {3, 0.1, 0.1}}, 0.075]},
 Axes → True, ImageSize → {300, 300}]
```

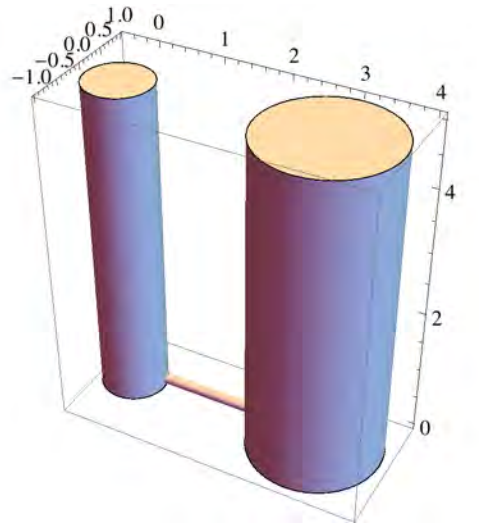

Formalizing the System

It is possible to formalize the system below by defining three functions: the transfer function $\tau_1(x)$, the buffering function $\beta_1(x)$, and the sigma function $\sigma_1(x)$.

The transfer function defines the amount of fluid present in the transfer vessel.

```
τ1[x_] := x / 5
```

Likewise, the buffering function defines the amount of fluid present in the buffering vessel.

```
β1[x_] := 4 x / 5
```

The sigma function defines the sum of the individual functions comprising the system.

```
σ1[x_] := τ1[x] + β1[x]
```

Once the functions are defined, it is possible to visualize the system by plotting the lines.

```
Plot[{σ1[x], β1[x], τ1[x]}, {x, 0, 100},
 AxesLabel → {"Total Volume", "Partial Volume"},
 PlotLegends → "Expressions"]
```

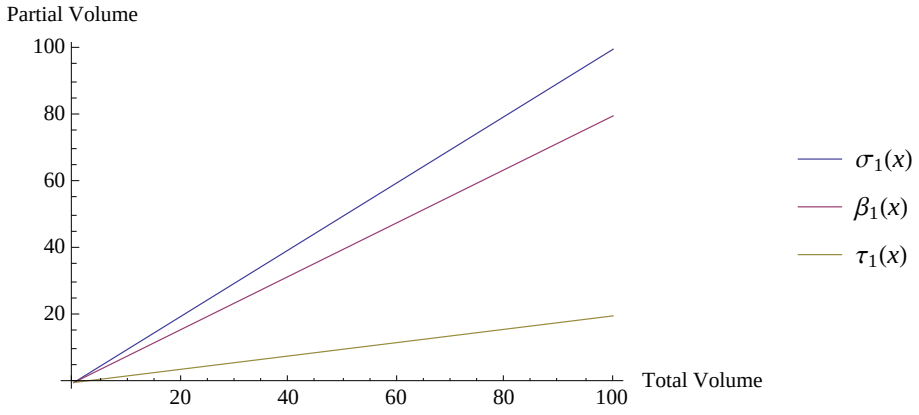

It is also possible to visualize the system (in a more intuitive manner) by creating an area plot in which the two partial volumes are indicated by the heights of the transfer and buffering areas at any given value of *x*.

```
Plot[{τ1[x], σ1[x]}, {x, 0, 100},
 AxesLabel → {"Total\nVolume", "Partial\nVolume"},
 Filling → Bottom,
 Epilog → {
   Text[TraditionalForm@HoldForm[β1[x]], {90, 50}],
   Text[TraditionalForm@HoldForm[τ1[x]], {90, 10}],
   Arrowheads[{-.03, .03}],
   Arrow[{{80, 0}, {80, τ1[80]}}],
   Arrow[{{80, τ1[80]}, {80, σ1[80]}}]
  }
]
```

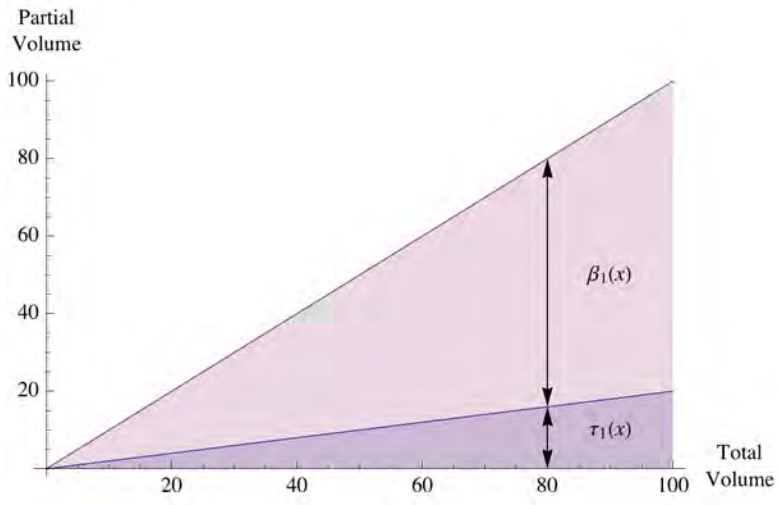

Defining the Buffering Parameters

The definition of the respective functions also provides a convenient means with which to quantitate buffering action. This is accomplished in any one of four ways, using the three available differentials. The buffering coefficient b_1 measures the change in the buffering compartment relative to the total change.

```
b1 = D[β1[x]] / D[σ1[x]]
```

$$\frac{4}{5}$$

The buffering ratio B_1 measures the change in the buffering compartment relative to the change in the transfer compartment.

```
B1 = D[β1[x]] / D[τ1[x]]
```

```
4
```

Conversely, the transfer coefficient t_1 measures the change in the transfer compartment relative to the total change.

```
t1 = D[τ1[x]] / D[σ1[x]]
```

$$\frac{1}{5}$$

The transfer ratio T_1 measures the change in the transfer compartment relative to the buffering compartment.

```
T1 = D[τ1[x]] / D[β1[x]]
```

$$\frac{1}{4}$$

In this simple linear example—where the cross-sectional area of the buffering vessel is constant (i.e. does not vary with fluid level)—the dimensionless values of total volumes *b*, *B*, *t*, and *T* are invariant, equal to 0.8, 4, 0.20, and .0.25, respectively.

Defining the Buffering Angle

While of great utility, the parameters *B* and *T* are undefined in the case of perfect buffering or perfect transfer, respectively. To address this issue, it is possible to define an alternative measure, the buffering angle α, which is capable of representing any type of buffering without the introduction of discontinuities.

As described in [1], the buffering angle α can be defined by first creating a three-dimensional space curve of the system.

```
ParametricPlot3D[{D[x], D[τ1[x]], D[β1[x]]}, {x, 0, 100},
 AxesLabel → {x, y, z}]
```

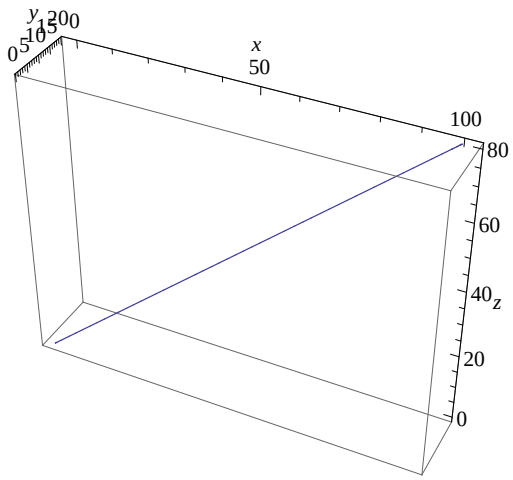

A projection of this curve onto the x-y plane corresponds to the transfer function.

```
ParametricPlot[{D[x], D[τ1[x]]}, {x, 0, 100},
 AxesLabel → {x, y}]
```

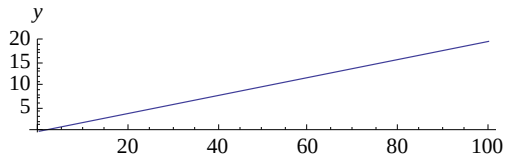

A projection onto the x-z plane corresponds to the buffering function.

```
ParametricPlot[{D[x], D[β1[x]]}, {x, 0, 100},
 AxesLabel → {x, z}]
```

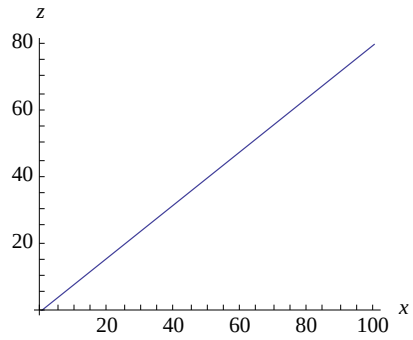

A projection onto the *y*-*z* plane, however, generates a third curve that can be used to determine the proportions between the individual changes in the transfer and buffering functions. This is accomplished by simply measuring the angle α_1 between the *y* axis and the line formed by joining the origin to any given point on the curve.

```
Module[{x, a, r},
 x = 20;
 a = ArcTan[D[τ1[x]], D[β1[x]]];
 r = Norm[{D[τ1[x]], D[β1[x]]}];
 ParametricPlot[{D[τ1[x]], D[β1[x]]}, {x, 0, 100},
  AxesLabel → {y, z}, ImageSize → 80 {1, 3},
  Epilog → {
    Circle[{0, 0}, r, {0, a}],
    Text["α1", r {Cos[1 / 2 a], Sin[1 / 2 a]},
     Background → White]
   }
 ]
]
```

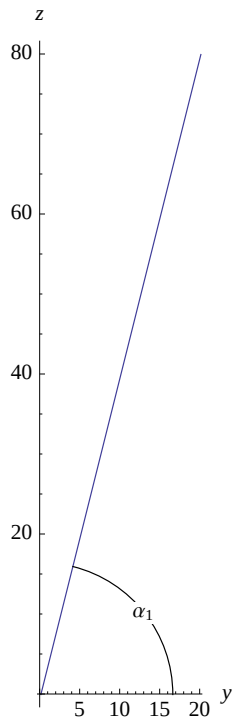

This calculates the buffering angle in degrees ([1], Supplement 5).

```
α1 = If[t1 ≤ 1, 1, -1] N[ArcCos[(t1 / √(t1^2 + b1^2))]] / Degree
```

```
75.9638
```

Similar to the buffering parameters, α_1 is invariant in cases of linear buffering.

```
Plot[α1, {x, 0, 100}, AxesLabel → {x, "α1"},
 PlotRange → {0, 90}]
```

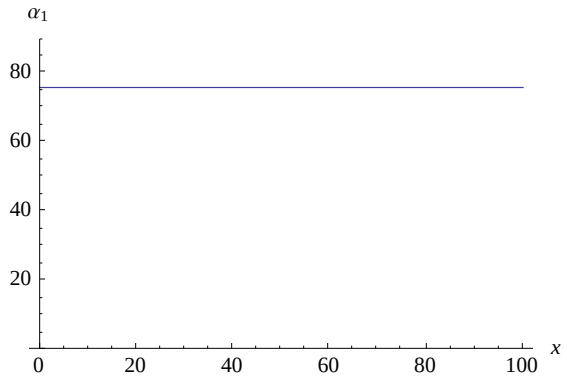

It is evident from the above analysis that this methodology creates a system in which perfect buffering corresponds to an angle of 90° and perfect transfer to an angle of 0°. In fact, any type of buffering behavior (moderating/amplifying/inverting/non-inverting) can be represented continuously by a finite angle between $-45°$ and 135° ([1], Supplement 7).

Importantly, it is also possible—using the same logic in the reverse direction—to use this single value to unambiguously define all of the buffering parameters describing the system. This can be demonstrated by defining a variable `littleb1` (corresponding to the buffering coefficient *b*) that is calculated using only the buffering angle.

```
littleb1 = Sin[α1 °] / (Cos[α1 °] + Sin[α1 °])
```

```
0.8
```

This checks that *b* and `littleb` are the same.

```
b1 == littleb1
```

```
True
```

Similarly, the values of the remaining three buffering parameters can be calculated using only the buffering angle and shown to be equal to the corresponding parameters calculated using the relevant differentials.

```
bigB1 = Sin[α1 °] / Cos[α1 °]
```

```
4.
```

```
B1 == bigB1
```

```
True
```

```
littlet1 = Cos[α1 °] / (Cos[α1 °] + Sin[α1 °])
```

```
0.2
```

```
t1 == littlet1
```

```
True
```

```
bigT1 = Cos[α1 °] / Sin[α1 °]
```

```
0.25
```

```
T1 == bigT1
```

```
True
```

Thus, the buffering angle provides a simple, powerful, single-value measure that is capable of capturing and communicating the underlying nature of the buffering relationships comprising the system.

A More Complex, Nonlinear Example

While the simple linear scenario described above made it possible to lay the foundation for Schmitt's "formal and general approach," the computational effort associated with its application was minimal. Thus, the utility of applying these methods within *Mathematica* was not fully exploited. For this reason, I next consider a more complex, nonlinear example (i.e. where the cross-sectional area of the buffering vessel is not constant). This serves the purpose of highlighting the advantages of exploiting *Mathematica*'s computational engine.

Defining a Nonlinear Buffering System

Consider a nonlinear system defined by the functions listed below.

```
τ2[x_] := 0.00395 x^11.09746 Exp[-2.30471 x]
```

```
σ2[x_] := x
```

```
β2[x_] := σ2[x] - τ2[x]
```

As previously described, the buffering parameters can be determined using the relevant differentials. However, in contrast to the previous example, the computational burden associated with their calculation is no longer trivial (at least in the absence of *Mathematica)*.

```
b2 = D[β2[x]] / D[σ2[x]]
```

$$\frac{x - 0.00395\, e^{-2.30471\, x}\, x^{11.0975}}{x}$$

```
B2 = D[β2[x]] / D[τ2[x]]
```

$$\frac{253.165\, e^{2.30471\, x}\, \left(x - 0.00395\, e^{-2.30471\, x}\, x^{11.0975}\right)}{x^{11.0975}}$$

```
t2 = D[τ2[x]] / D[σ2[x]]
```

$$0.00395\, e^{-2.30471\, x}\, x^{10.0975}$$

```
T2 = D[τ2[x]] / D[β2[x]]
```

$$\frac{0.00395\, e^{-2.30471\, x}\, x^{11.0975}}{x - 0.00395\, e^{-2.30471\, x}\, x^{11.0975}}$$

Once the functions are defined and the system visualized through the creation of the corresponding line and area plots, one can clearly see that the magnitude of buffering action in this nonlinear scenario varies with fluid level (imagine a buffering vessel in the shape of an hourglass as opposed to a cylinder).

```
Plot[{τ2[x], β2[x], σ2[x]}, {x, 0, 12},
 AxesLabel → {"Total\nVolume", "Partial\nVolume"},
 PlotLegends → "Expressions"]
```

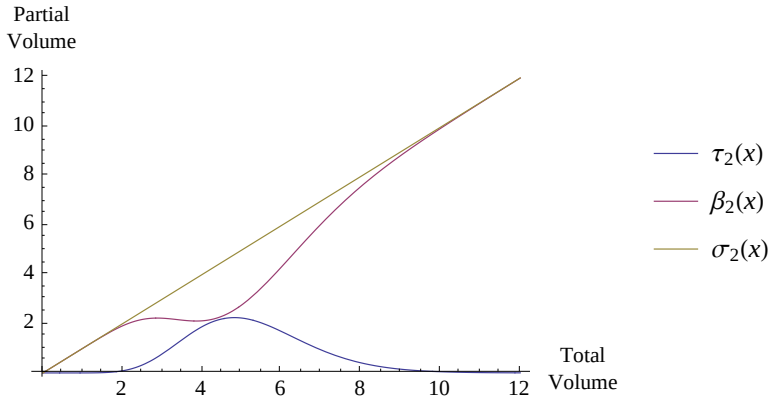


```
Plot[{τ2[x], σ2[x]}, {x, 0, 12}, Filling → Bottom,
 AxesLabel → {"Total\nVolume", "Partial\nVolume"},
 Epilog → {
   Text[HoldForm[β2[x]], {10, 5}],
   Text[HoldForm[τ2[x]], {5, 1}]
  }
]
```

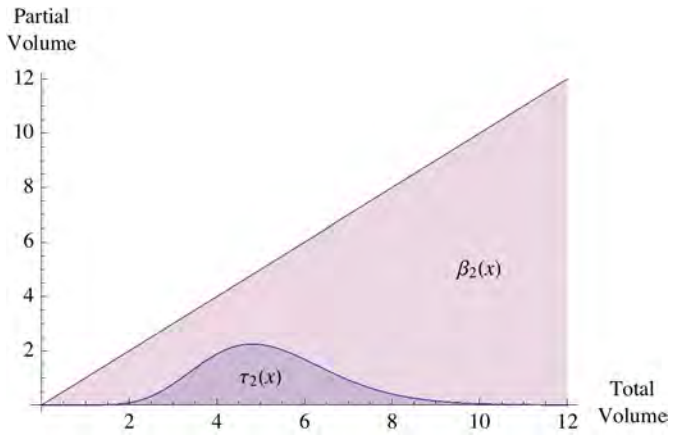

Furthermore, unlike the linear case, it is also clear that the buffering parameters vary as a function of *x*.

```
Plot[b2, {x, 0, 12}, PlotRange → {0, 2}, AxesLabel → {x, "b2"}]
```

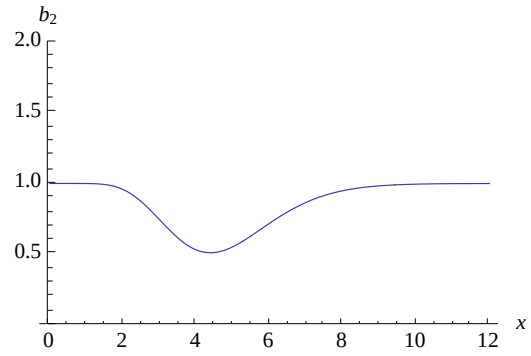


```
Plot[B2, {x, 0, 12}, PlotRange → {0, 20}, AxesLabel → {x, "B2"}]
```

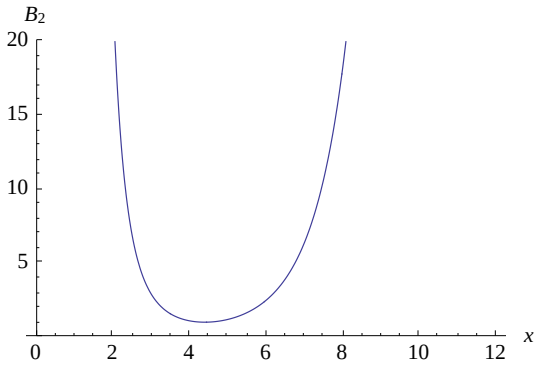


```
Plot[t2, {x, 0, 12}, PlotRange → {0, 0.5},
 AxesLabel → {x, "t2"}]
```

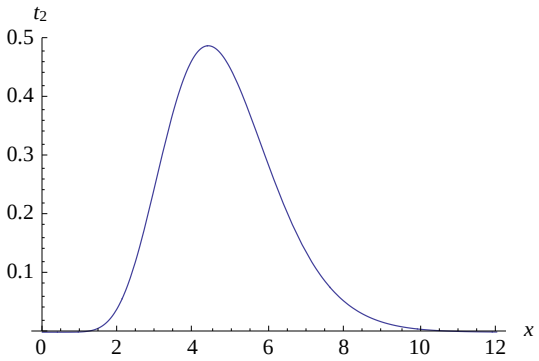

```
Plot[T₂, {x, 0, 12}, PlotRange → {0, 1}, AxesLabel → {x, "T₂"}]
```

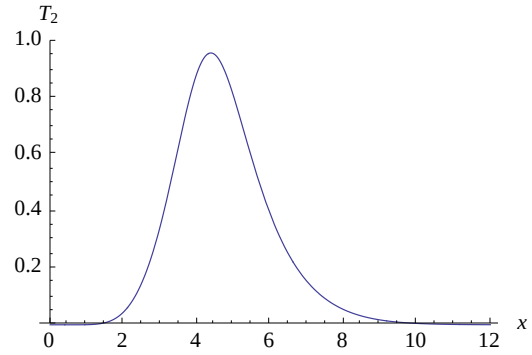

Defining the Buffering Angle of a Nonlinear System

As previously described, it is also possible to calculate the buffering angle α_2 by first creating a three-dimensional space curve of the system and then projecting this curve onto the *y*-*z* plane.

```
ParametricPlot3D[{D[x], D[τ₂[x]], D[β₂[x]]}, {x, 0, 12},
 AxesLabel → {x, y, z}]
```

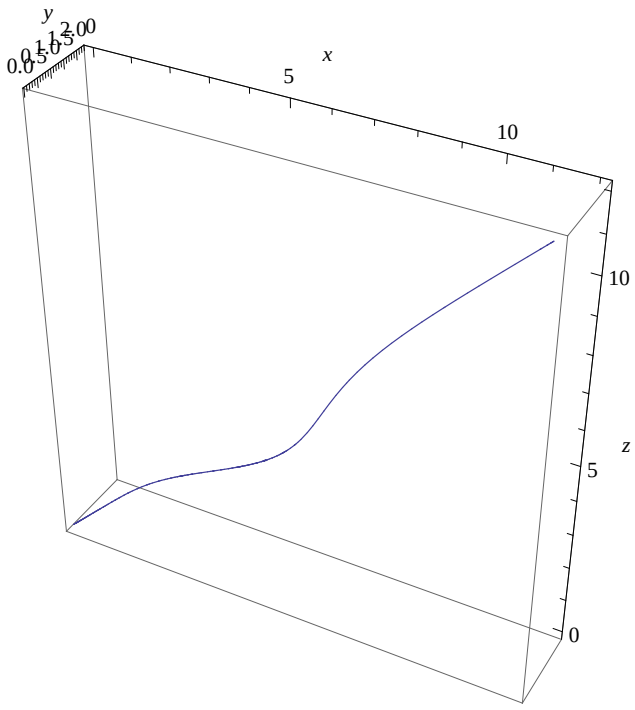

```
Module[{x, p, a, r},
 x = 4;
 p = {D[τ2[x]], D[β2[x]]};
 a = ArcTan[D[τ2[x]], D[β2[x]]];
 r = Norm[{D[τ2[x]], D[β2[x]]}];
 ParametricPlot[{D[τ2[x]], D[β2[x]]}, {x, 0, 12},
  AxesLabel → {y, z}, ImageSize → 100 {1.25, 5.5},
  Epilog → {
    {Orange, Circle[{0, 0}, .5 r, {0, a}]},
    Text[Row[{"α2", "(", Style["x", Italic], ")"}],
     .5 r {Cos[1 / 2 a], Sin[1 / 2 a]}, Background → White],
    Thickness[.02], Orange, Line[{{0, 0}, p}],
    PointSize[.07], Point[p]
   }
 ]
]
```

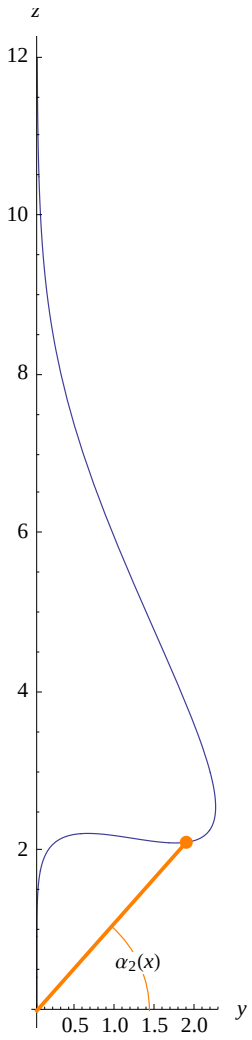

In this instance the buffering angle α_2 varies as a function of x, with near-perfect buffering being observed at both high and low fluid levels, and minimal buffering being observed when x attains a value of approximately 4.38.

```
α2 = If[t2 ≤ 1, 1, -1] N[ArcCos[(t2 / √(t2^2 + b2^2))]] / Degree
```

```
1/° ArcCos[(0.00395 × 2.71828^(-2.30471 x) x^10.0975) /
    (√((0.0000156025 × 2.71828^(-4.60942 x) x^20.1949 +
        (x - 0.00395 × 2.71828^(-2.30471 x) x^11.0975)^2 / x^2)))]
  If[0.00395 ℯ^(-2.30471 x) x^10.0975 ≤ 1, 1, -1]
```

```
Plot[α2, {x, 0, 12}, AxesLabel → {x, "α2"}, PlotRange → {0, 90}]
```

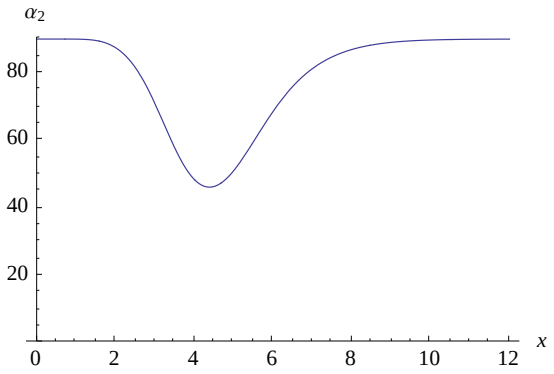

As described previously, the buffering parameters can be determined using the buffering angle and are equivalent to the values calculated using the originally defined functions (compare the plots below to the plots for b_1, B_1, t_1, and T_1 above).

```
littleb2 = Sin[α2 °] / (Cos[α2 °] + Sin[α2 °]);
```

```
Plot[littleb2, {x, 0, 12}, PlotRange → {0, 2},
 AxesLabel → {x, "littleb2"}]
```

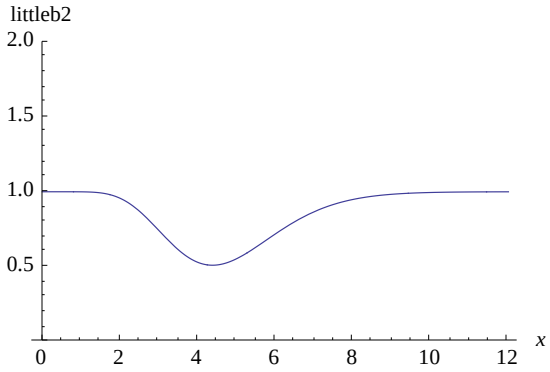


```
bigB2 = (Sin[α2 °] / Cos[α2 °]);
```

```
Plot[bigB2, {x, 0, 12}, PlotRange → {0, 20},
 AxesLabel → {x, "bigB2"}]
```

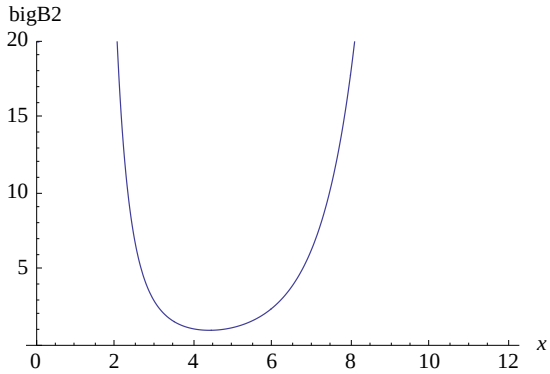


```
littlet2 = Cos[α2 °] / (Cos[α2 °] + Sin[α2 °]);
```

```
Plot[littlet2, {x, 0, 12}, PlotRange → {0, 0.5},
 AxesLabel → {x, "littlet2"}]
```

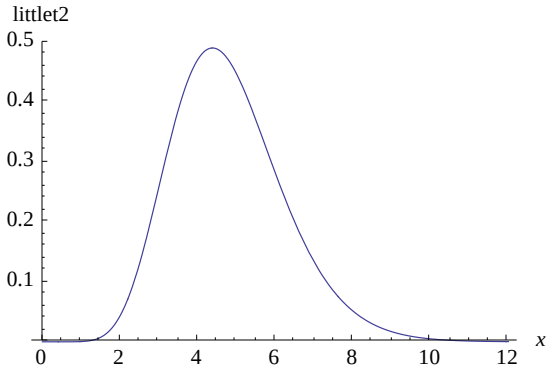


```
bigT2 = (Cos[α2 °] / Sin[α2 °]);
```

```
Plot[bigT2, {x, 0, 12}, PlotRange → {0, 1},
 AxesLabel → {x, "bigT2"}]
```

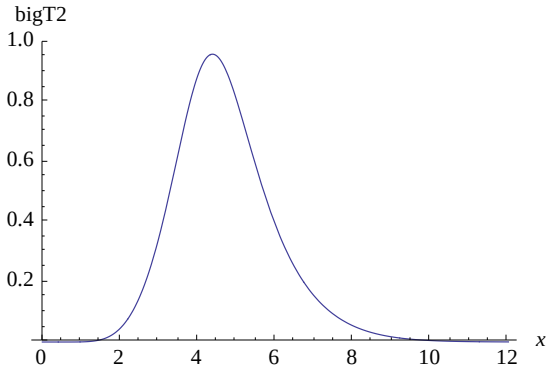

Thus, just as in the case of a linear system, plotting α_2 over the range of the disturbance (i.e. the addition of fluid) provides a simple, single-value measure with which to grasp the inherent buffering properties of the system under consideration.

Differentials versus Derivatives

At this point it is important to note that, up to now, only the overall changes in the buffering and transfer compartments have been considered (by comparing differentials). However, in the case of nonlinear systems, it is also informative to consider the *rate* at which these values change relative to one another (by comparing derivatives). For example, in the same way that it would be important for an investor to be aware of the current price of gold, and how it has changed in previous years, months, or weeks, it would also be important for that same investor to be cognizant of the rate at which the price is changing at any given instant in time (i.e. increasing, decreasing, or stable). This is to say, the choice to sell at a given price at a given moment would be greatly influenced by knowing if the price was stable or on either an upward or a downward trend. In other words, it is not only of interest to know how a quantity *has changed*, but how that quantity *is changing*.

To determine the instantaneous rates of change in a buffered system, simply calculate and plot the first derivatives of the functions describing the system.

```
D[β2'[x]]
```

$$1 - 0.043835\, e^{-2.30471\, x}\, x^{10.0975} + 0.0091036\, e^{-2.30471\, x}\, x^{11.0975}$$

```
D[τ2'[x]]
```

$$0.043835\, e^{-2.30471\, x}\, x^{10.0975} - 0.0091036\, e^{-2.30471\, x}\, x^{11.0975}$$

```
D[σ2'[x]]
```

```
1
```

```
Plot[{τ2'[x], β2'[x], σ2'[x]}, {x, 0, 12},
 AxesLabel → {"Total\nVolume", "Rate of\nChange"},
 PlotLegends → "Expressions"]
```

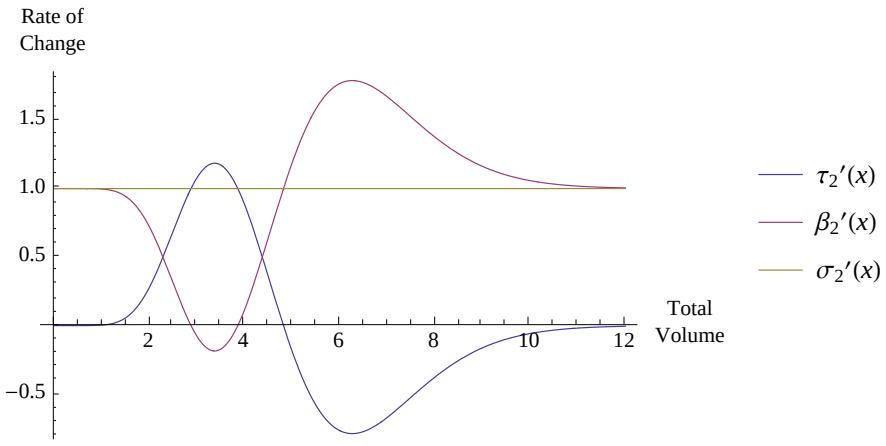

Once the functions are defined, the instantaneous buffering parameters (denoted by adding an "i" to the respective variable names) can also be calculated.

```
b2i = D[β2'[x]] / D[σ2'[x]]
```

$$1 - 0.043835\, e^{-2.30471\, x}\, x^{10.0975} + 0.0091036\, e^{-2.30471\, x}\, x^{11.0975}$$

```
B2i = D[β2'[x]] / D[τ2'[x]]
```

$$\left(1 - 0.043835\, e^{-2.30471\, x}\, x^{10.0975} + 0.0091036\, e^{-2.30471\, x}\, x^{11.0975}\right) \Big/ \left(0.043835\, e^{-2.30471\, x}\, x^{10.0975} - 0.0091036\, e^{-2.30471\, x}\, x^{11.0975}\right)$$

```
t2i = D[τ2'[x]] / D[σ2'[x]]
```

$$0.043835\, e^{-2.30471\, x}\, x^{10.0975} - 0.0091036\, e^{-2.30471\, x}\, x^{11.0975}$$

```
T2i = D[τ2'[x]] / D[β2'[x]]
```

$$\left(0.043835\, e^{-2.30471\, x}\, x^{10.0975} - 0.0091036\, e^{-2.30471\, x}\, x^{11.0975}\right) \Big/ \left(1 - 0.043835\, e^{-2.30471\, x}\, x^{10.0975} + 0.0091036\, e^{-2.30471\, x}\, x^{11.0975}\right)$$

As is evident from viewing the respective plots of these functions, this analysis allows one to clearly identify the points of maximum and minimum buffering/transfer rate, as well as the points at which the buffering/transfer rates are zero.

```
Plot[b2i, {x, 0, 12}, PlotRange → {-1, 2},
 AxesLabel → {"Total\nVolume", HoldForm[β2'[x] / σ2'[x]] }]
```

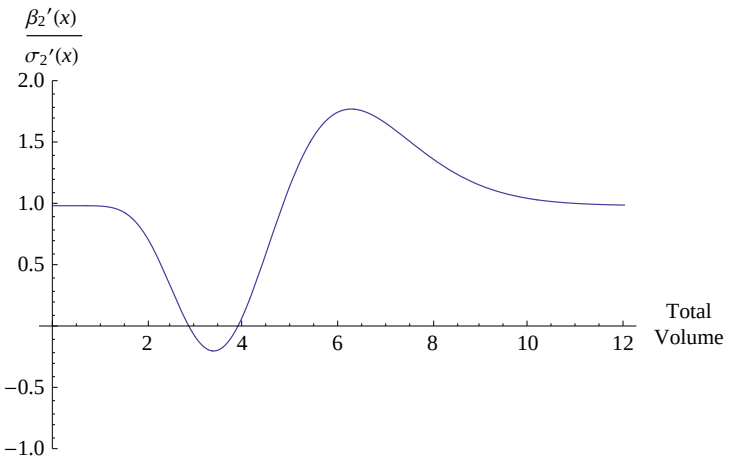

```
Plot[t2i, {x, 0, 12}, PlotRange → {-1.5, 1.5},
 AxesLabel → {"Total\nVolume", HoldForm[τ2'[x] / σ2'[x]]}]
```

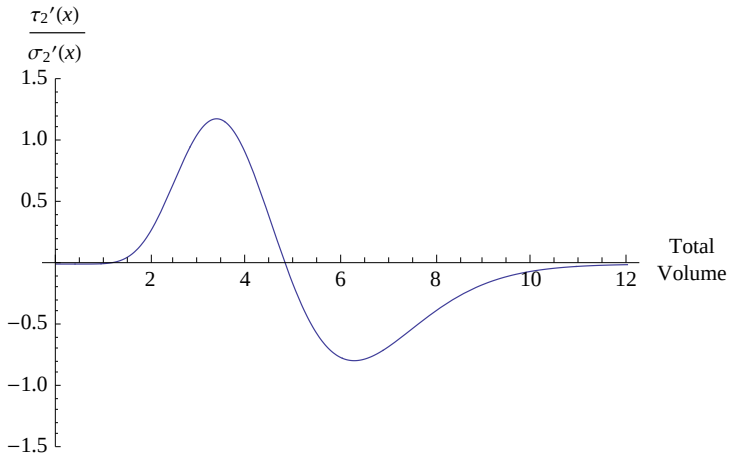


```
Plot[T2i, {x, 0, 12}, PlotRange → {-20, 20},
 AxesLabel → {"Total\nVolume", HoldForm[τ2'[x] / β2'[x]]}]
```

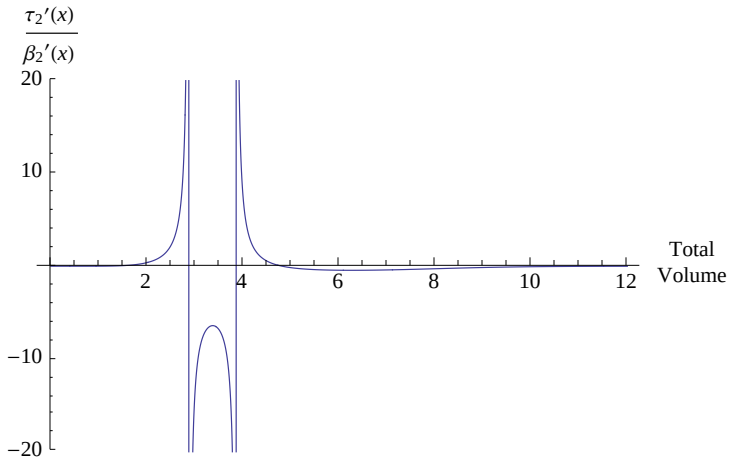

In this way, the most critical junctures in the development of the system (over the range of the disturbance) can be quickly and easily identified.

From the Abstract to the Practical

The analysis presented in the previous sections concludes my efforts to establish the theoretical foundation of the formal and general approach, as well as its application within *Mathematica*. Next, in order to illustrate how these abstractions can be directly applied to the real world, I consider an example of non-classical buffering—namely, that of the "genetic buffering" of phenotypic variation. In this way, the ability to exactly and formally quantitate phenomena that at first glance might be thought of as being outside the buffering paradigm is practically demonstrated.

Genetic Buffering

The axiomatic foundation and abstract nature of the "formal and general approach" allows it to be readily applied to any scenario in which an arbitrary quantity partitions itself between two compartments or states. While suitable for the analysis of "classical" buffering phenomena (the homeostasis of physiological parameters), the approach is also germane to a variety of "non-classical" buffering phenomena. One such phenomenon, which up to now has been considered in only a qualitative manner, is that of "genetic" buffering. While many instances of genetic buffering have been described and characterized, a well-known and classic example of the phenomenon—revolving around the gene encoding the heat shock protein Hsp90—will be used to illustrate the real-world application of Schmitt's paradigm.

The Heat Shock Protein Hsp90

The Hsp90 protein is an ATP-dependent molecular "chaperone" that is extensively expressed in organisms ranging from bacteria to humans. It functions to promote the proper folding of a specific subset of molecular targets referred to as its "client" proteins. Interestingly, many of Hsp90's client proteins are involved in the process of signal transduction and modulate developmental processes [3]. For example, in the fruit fly, *Drosophila melanogaster*, mutations in the gene encoding Hsp90 result in morphological abnormalities affecting the development of the eye, legs, wings, thorax, and bristles [4].

Interestingly, the proportion of Hsp90 mutant flies exhibiting eye defects (in a line prone to such abnormalities) increases dramatically as the temperature rises. In contrast, the proportion of control flies (expressing the normal or "wild-type" version of the Hsp90 protein) also increases in response to increased temperature, but not nearly to the same degree as in the mutant flies [4]. The gene encoding the wild-type version of the Hsp90 protein is thus said to "buffer" the appearance of the defective eye trait.

■ *Formally Quantitating Hsp90-Mediated Buffering of Phenotypic Variation*

It is possible to analyze these experimental results in more detail by importing the raw data (see Figure 8 in [4]) from the original publication in the form of two arrays. These two arrays, corresponding to the wild-type and mutant fly lines, relate temperature to the penetrance of the mutant phenotype (i.e. the percentage of flies in the line displaying the eye defect).

```
wildtypeHsp90 = {{18, 0}, {21, 0}, {25, 0}, {26, 1},
  {27, 3}, {30, 19}, {32, 16}}
```

```
{{18, 0}, {21, 0}, {25, 0},
 {26, 1}, {27, 3}, {30, 19}, {32, 16}}
```

```
mutantHsp90 = {{18, 2}, {21, 10}, {25, 10}, {26, 25},
  {27, 45}, {30, 70}, {32, 82}}
```

```
{{18, 2}, {21, 10}, {25, 10},
 {26, 25}, {27, 45}, {30, 70}, {32, 82}}
```

Plotting the data illustrates that the mutant line is indeed more sensitive to increasing temperature than the wild-type line.

```
Show[ListPlot[mutantHsp90, PlotStyle → Red,
  PlotMarkers → Automatic,
  AxesLabel → {"Temperature (°C)", "Affected (%)"},
  PlotRange → {-1, 100}],
 ListPlot[wildtypeHsp90, PlotStyle → Darker@Green,
  PlotMarkers → Automatic]]
```

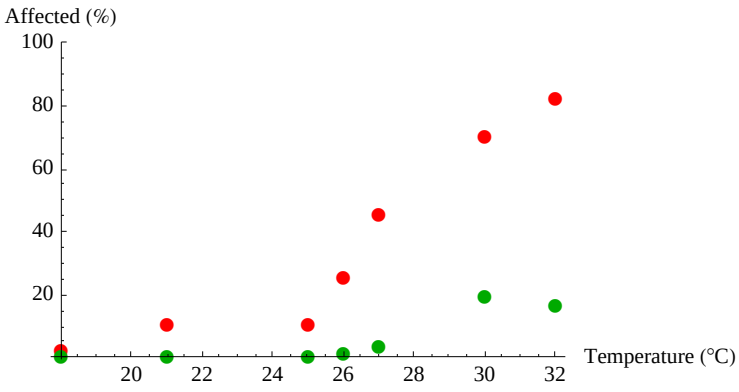

To proceed with the application of the formal and general approach, we now create two curves that fit the data using the `FindFit` function.

```
FindFit[wildtypeHsp90, j Exp[-k X], {j, k}, X,
 Method → NMinimize]
```

```
{j → 0.0031044, k → -0.272652}
```

```
FindFit[mutantHsp90, j Exp[-k X], {j, k}, X,
 Method → NMinimize]
```

```
{j → 0.193965, k → -0.191242}
```

With the above constants, the curves describing the behavior of the wild-type and mutant lines can be generated.

```
wildtypecurve[x_] :=
 j Exp[-k x] /. FindFit[wildtypeHsp90, j Exp[-k X],
    {j, k}, X, Method → NMinimize]
```

```
mutantcurve[x_] :=
 j Exp[-k x] /. FindFit[mutantHsp90, j Exp[-k X], {j, k},
    X, Method → NMinimize]
```

```
wildtypecurve[x]
```

$$0.0031044\, e^{0.272652\, x}$$

```
mutantcurve[x]
```

$$0.193965\, e^{0.191242\, x}$$

The appropriateness of the fit can then be inspected by plotting the curves together with the raw data.

```
Show[
 ListPlot[mutantHsp90, PlotStyle → Red,
  PlotMarkers → Automatic,
  AxesLabel → {"Temperature (°C)", "Affected (%)"}],
 ListPlot[wildtypeHsp90, PlotStyle → Darker@Green,
  PlotMarkers → Automatic],
 Plot[Evaluate[{mutantcurve[x], wildtypecurve[x]}],
  {x, 18, 32}, PlotStyle → {Red, Darker@Green}]
]
```

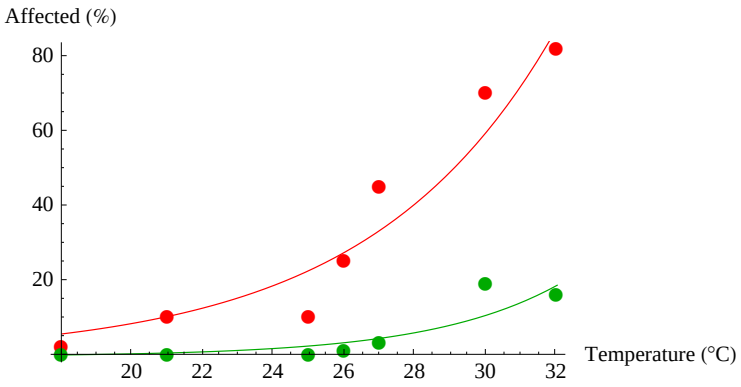

With these results in hand, it is now possible to define both the buffering and transfer functions and then to visualize the system using an area plot.

```
τ3[x_] := Evaluate[wildtypecurve[x]]
```

```
β3[x_] := Evaluate[mutantcurve[x]]
```

```
σ3[x_] := τ3[x] + β3[x]
```

```
Plot[{τ3[x], σ3[x]}, {x, 18, 32}, Filling → Bottom,
 AxesLabel → {"Temperature (°C)", "Affected (%)"},
 Epilog → {
   Text[HoldForm[β3[x]], {31, 40}],
   Text[HoldForm[τ3[x]], {31, 7}]
  }
]
```

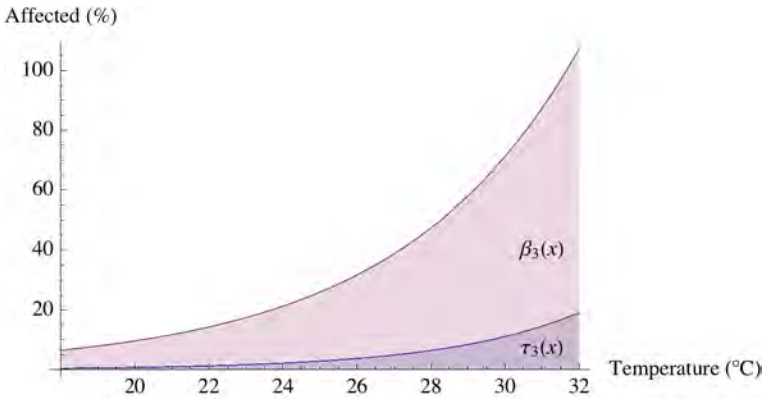

As is evident from inspecting this plot, an increase in temperature translates into only a small increase in the proportion of flies with eye defects in the wild-type line. However, in the mutant line, a much more pronounced increase is observed. We can thus infer that the expression of the wild-type Hsp90 protein buffers the effect of temperature on the penetrance of the eye defect. In other words, since the "transfer" of the eye defect phenotype is greater in the mutant line, the wild-type Hsp90 protein must possess the abstract capacity of diverting or "soaking up" this disturbance (into an equally abstract buffering compartment) so that the "transfer" of the eye defect is diminished. Importantly, using the formal and general approach, we can now provide an exact quantitative measure of the buffering capacity of the wild-type allele by calculating and plotting the four buffering parameters together with the buffering angle (below).

```
b3 = D[β3[x]] / D[σ3[x]]
```

$$\frac{0.193965\, e^{0.191242\, x}}{0.193965\, e^{0.191242\, x} + 0.0031044\, e^{0.272652\, x}}$$

```
Plot[b3, {x, 18, 32}, PlotRange → {.8, 1},
 AxesLabel → {"Temperature (°C)", "b3"}]
```

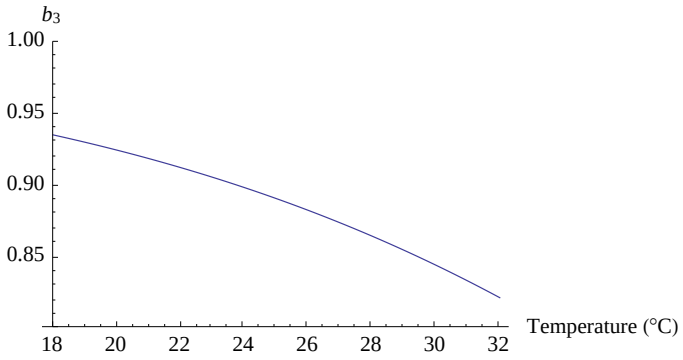


```
B3 = D[β3[x]] / D[τ3[x]]
```

$$62.4808\, e^{-0.0814101\, x}$$

```
Plot[B3, {x, 18, 32}, PlotRange → {4, 16},
 AxesLabel → {"Temperature (°C)", "B3"}]
```

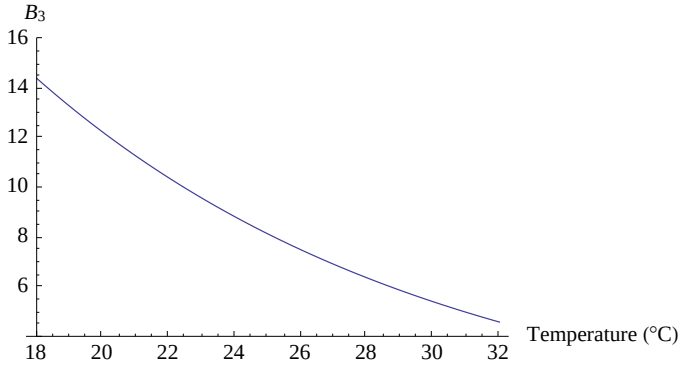


```
t3 = D[τ3[x]] / D[σ3[x]]
```

$$\frac{0.0031044\, e^{0.272652\, x}}{0.193965\, e^{0.191242\, x} + 0.0031044\, e^{0.272652\, x}}$$

```
Plot[t3, {x, 18, 32}, AxesLabel → {"Temperature (°C)", "t3"}]
```

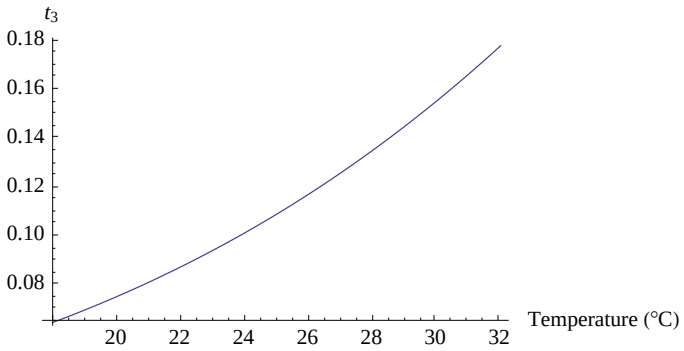


```
T3 = D[τ3[x]] / D[β3[x]]
```

$$0.0160049\, e^{0.0814101\, x}$$

```
Plot[T3, {x, 18, 32}, AxesLabel → {"Temperature (°C)", "T3"}]
```

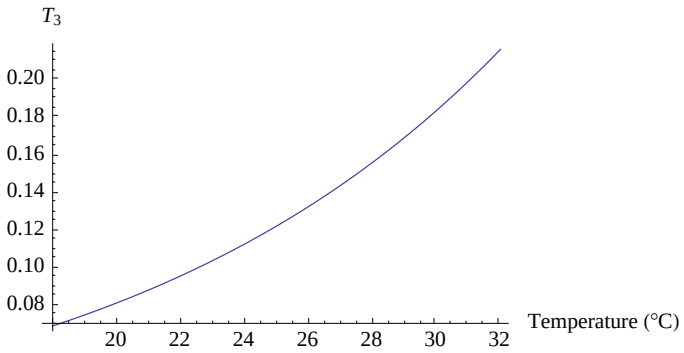


```
α3 = If[t3 ≤ 1, 1, -1] N[ArcCos[(t3 / √(t3^2 + b3^2))]] / Degree;
```

```
Plot[α3, {x, 18, 32}, AxesLabel → {"Temperature (°C)", "α3"}]
```

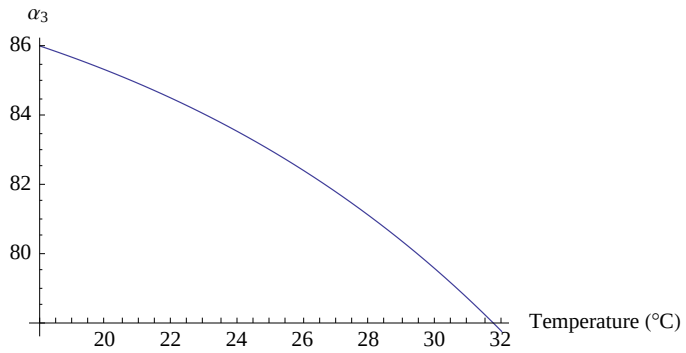

As shown above, the buffering coefficient b_3 can be calculated to range from ~0.935 at 18 °C to ~0.822 at 32 °C. While these calculations are now trivial, the critical biological question of how to interpret these calculations is more challenging. As discussed by Schmitt ([1], Supplements 6 and 7), one way to proceed is to consider the conceptual overlap between the formal and general approach and probability theory. In essence, the buffering coefficient b_3 is analogous to a probability. In the same way that a probability measures the proportion of a part to a whole (i.e. the number of successful events to the total number of events), so does the buffering coefficient (by measuring the fractional change in the buffering compartment relative to the whole compartment). The critical realization is that both quantities are measured on a relative scale that is normalized to 1. Interpreting the graph in this way, one can say that the "probability" of buffering decreases from ~0.935 to ~0.822 from 18 °C to 32 °C.

Using similar logic, one can say that, in essence, the buffering ratio B_3 is analogous to the "odds" of buffering. In the same way that odds measure the proportion between two parts of a whole (by comparing events to non-events), so does B_3 (by comparing the fractional change in the buffering compartment to the fractional change in the transfer compartment). Again the critical realization is that both quantities are measured on a scale with equal intervals and an absolute zero. Interpreting the data in this way, one can say that the "odds" of buffering decrease from ~14.4 to ~4.6 from 18 °C to 32 °C. Similarly, one can consider t_3 and T_3 to be analogous to the "probability" of transfer and the "odds" of transfer, respectively.

Lastly, the buffering angle provides information regarding not only the magnitude of buffering but also the class of buffering behavior. As discussed by Schmitt ([1], Supplement 7), angles between 90° and 0° correspond to non-inverting moderation, with angles of 90° corresponding to perfect buffering and 0° to zero buffering. Thus, the simple inspection of the plot of α_3 reveals that the buffering capacity of wild-type Hsp90 is very strong (near perfect at ~86°) but decreases slightly with increasing temperature (to a value of ~78°). In any event—and however the data is interpreted—the analysis presented above clearly demonstrates the ease with which the buffering capacity of a genetic determinant can be formally and exactly quantified.

Conclusion

A formal conceptualization of genetic buffering was first put forward by famed geneticist and Nobel laureate Leland Hartwell [5, 6]. In these publications, Hartwell highlights the importance of buffering relationships in determining phenotype in outbred organisms. Subsequent research both in yeast and in the roundworm, *Caenorhabditis elegans*, has strongly supported his assumptions [7, 8]. Thus, in addition to increasing our basic understanding of genetic networks, these results also raised the theoretical question of whether or not it might be possible to provide an exact quantitative measure of a genetic determinant's buffering activity.

As described for the first time above, Schmitt's "formal and general approach" provides a powerful means with which to accomplish this goal. Through the calculation of the four buffering parameters b, B, t, and T and the buffering angle α, it is indeed possible to provide an exact quantitative measure of the buffering activity or "power" of any genetic determinant in response to an environmental disturbance. Furthermore, the activity can be measured using either a relative scale normalized to one (b and t) or an absolute scale with equal intervals (B and T), or distilled to a single value measure α, capable of describing the system in its entirety.

In conclusion, it must be noted that the application of the formal and general approach becomes practical only when used in conjunction with a sophisticated computational engine that is capable of readily analyzing the relevant data. As demonstrated in this article, *Mathematica* provides such an engine. The application of the formal and general approach using the Wolfram Language thus provides a powerful tool with which to quantitatively analyze both classical and non-classical buffering phenomena, irrespective of discipline.

References

[1] B. M. Schmitt, "The Quantitation of Buffering Action I. A Formal & General Approach," *Theoretical Biology and Medical Modelling*, **2**(8), 2005. doi:10.1186/1742-4682-2-8.

[2] B. M. Schmitt, "The Quantitation of Buffering Action II. Applications of the Formal & General Approach," *Theoretical Biology and Medical Modelling*, **2**(9), 2005. doi:10.1186/1742-4682-2-9.

[3] M. Taipale, D. F. Jarosz, and S. Lindquist, "HSP90 at the Hub of Protein Homeostasis: Emerging Mechanistic Insights," *Nature Reviews Molecular Cell Biology*, **11**(7), 2010 pp. 515–528. doi:10.1038/nrm2918.

[4] S. L. Rutherford and S. Lindquist, "Hsp90 as a Capacitor for Morphological Evolution," *Nature*, **396**, 1998 pp. 336–342. doi:10.1038/24550.

[5] J. L. Hartman, B. Garvik, and L. Hartwell, "Principles for the Buffering of Genetic Variation," *Science*, **291**(5506), 2001 pp. 1001–1004. www.sciencemag.org/content/291/5506/1001.abstract.

[6] L. Hartwell, "Robust Interactions," *Science*, **303**(5659), 2004 pp. 774–775. doi:10.1126/science.1094731.

[7] A. H. Tong, G. Lesage, G. D. Bader, H. Ding, H. Xu, X. Xin, J. Young, G. F. Berriz, R. L. Brost, M. Chang, Y. Chen, X. Cheng, G. Chua, H. Friesen, D. S. Goldberg, J. Haynes, C. Humphries, G. He, S. Hussein, L. Ke, N. Krogan, Z. Li, J. N. Levinson, H. Lu, P. Ménard, C. Munyana, A. B. Parsons, O. Ryan, R. Tonikian, T. Roberts, A. M. Sdicu, J. Shapiro, B. Sheikh, B. Suter, S. L. Wong, L. V. Zhang, H. Zhu, C. G. Burd, S. Munro, C. Sander, J. Rine, J. Greenblatt, M. Peter, A. Bretscher, G. Bell, F. P. Roth, G. W. Brown, B. Andrews, H. Bussey, and C. Boone, "Global Mapping of the Yeast Genetic Interaction Network," *Science*, **303**(5659), 2004 pp. 808–813. doi:10.1126/science.1091317.

[8] B. Lehner, C. Crombie, J. Tischler, A. Fortunato, and A. G. Fraser, " Systematic Mapping of Genetic Interactions in *Caenorhabditis Elegans* Identifies Common Modifiers of Diverse Signaling Pathways," *Nature Genetics*, **38**(8), 2006 pp. 896–903. doi:10.1038/ng1844.

J. Karagiannis, "The Quantitation of Non-classical Buffering," *The Mathematica Journal*, 2015. dx.doi.org/doi:10.3888/tmj.17-3.

About the Author

Dr. Jim Karagiannis is an associate professor at the University of Western Ontario in London, Ontario, Canada. His research makes use of the model eukaryote *Schizosaccharomyces pombe* and explores the complex post-translational modifications that take place on the carboxy-terminal domain (CTD) of the largest subunit of RNA polymerase II. Through an empirical examination of the informational properties and regulatory potential of the CTD, Dr. Karagiannis hopes to decipher the "programming language" used by eukaryotes to control aspects of gene expression.

Jim Karagiannis
Department of Biology
The University of Western Ontario
London, ON
Canada, N6A-5B7
jkaragia@uwo.ca